

Unveiling the role of chemical and electronic structure in plasmon-assisted homolysis of alkoxyamines

Daria Votkina¹, Pavel Petunin¹, Elena Miliutina², Andrii Trelin², Oleksiy Lyutakov², Vaclav Svorcik²,
G rard Audran³, Jeffrey Havot³, Rashid Valiev^{1,5}, Lenara I. Valiulina,⁴ Jean-Patrick Joly³, Olga
Guselnikova^{1,2}* Sylvain R. A. Marque^{3*} and Pavel Postnikov^{1,2*}

¹ *Research School of Chemistry and Applied Biomedical Sciences, Tomsk Polytechnic University, Russian Federation*

² *Department of Solid-State Engineering, University of Chemistry and Technology, Prague, Czech Republic*

³ *Aix-Marseille Univ, CNRS, ICR case 551, Avenue Escadrille Normandie-Niemen, 13397 Marseille Cedex 20, France*

⁴ *Tomsk State University, 36, Lenin Avenue, 634050 Tomsk, Russia*

⁵ *University of Helsinki, Department of Chemistry, P.O. Box 55, (A.I. Virtanens plats 1), FIN-00014 University of Helsinki, Finland*

Abstract

The excitation of localized plasmon resonance on nanoparticles followed by the interaction with organic molecules leads to new pathways of chemical reactions. Although a number of physical factors (temperature, illumination regime, type of nanoparticles, etc.) are affecting this process, the role of the chemical factors is underestimated. Challenging this assumption, here we studied the kinetic of plasmon-induced homolysis of five alkoxyamines (AAs) with different chemical and electronic structures using electron paramagnetic resonance (EPR). The kinetic data revealed the dependence of plasmonic homolysis rate constant (k_d) with the HOMO energy of AAs, which cannot be described by the kinetic parameters

derived from thermal homolysis experiments. The observed trend in k_d allowed to suggest the key role of intramolecular excitation mechanism supported by the TDFDT calculations, additional spectroscopic characterization, and control experiments. Our work sheds light on the role of the electronic structure of organic molecules in plasmonic chemistry.

Keywords: plasmon, homolysis, alkoxyamines, plasmon-driven reaction, photocatalysis

Introduction

Recently we learned that chemical transformation could be driven using the energy of plasmon resonance excitation as an alternative to classical catalytic approaches^{1,2}. Plasmon-active substrates (Au, Ag, Cu, Pt) are illuminated with a light source leading to the energy generation transformed to the energy required for the activation of molecules. Originally, the plasmonic approach was successfully applied toward enhancing catalysis of inorganic reactions such as CO/CO₂ reduction or water splitting^{3,4}, but organic reactions could not shot out for a long⁵. The utilization of plasmon catalysis opens a huge potential for improved selectivity^{6,7}, enhanced reaction rates^{8,9}, and milder reaction conditions¹⁰. Up to now, the range of plasmon-assisted organic reactions was reported, such as oxidation of alcohols, amines, and unsaturated compounds; reductive transformations; C–C and C–N bond formation; and polymerization⁵. Despite the diversity of reactions, mechanisms and fundamental principles^{11,12} are investigated using model reactions such as dimerization of *p*-amino/nitro thiophenol.

The mechanism of interaction between plasmon and organic molecules is still disputable. Nowadays, three main hypotheses have been proposed: (1) reaction acceleration through plasmonic heating, (2) transfer of «hot» carriers to the organic molecule, followed by the formation and relaxation of the excited state; (3) intramolecular excitation of an electron to the LUMO via the decay of the optically excited surface plasmon (SP).^{13,14} All these processes, benefited from plasmonic metal nanostructures, can impel plasmonic chemistry. However, recent studies^{13, 14,15} including ours^{8,10} cast a doubt on mechanisms (1) and (2) but provide more evidence about intramolecular excitation process (3) in some cases.

The intramolecular excitation mechanism was also adapted for the hybrid plasmonic substrates to manipulate the energy of excited states via the hybridization between the electronic structures of metals/semiconductors with the molecular orbitals of organic reagents.^{16,17} However, none of the theories is considering in detail the effects of the electronic structure of organic molecules on the processes of plasmon-induced transformations. In our recent study using alkoxyamines as a perfect thermal probe for plasmon catalysis (due to 1st order, one component reaction), we unveiled the effect of the nature of the organic

molecule on the plasmonic kinetic. We have demonstrated that alkoxyamines (AAs) $R_1R_2NOR_3$ are molecules that homolyze into nitroxides ($R_1R_2NO\bullet$) and reactive alkyl radicals ($R_3\bullet$), can be monitored by precise EPR measurements, under plasmon excitation on the gold surface.^{10,18} Thus, there is a genuine need, from both fundamental and applied viewpoints, to elucidate the role of the nature/structure of molecules and their electronic structure to the plasmonic chemistry. Filling this gap promises to unlock an unprecedented control over kinetic and thermodynamic parameters of organic reactions and to carefully develop the plasmonic catalysts for organic transformations.

Here, using the advantages of AAs, we performed a thorough study on the kinetic of the plasmon-induced homolysis of alkoxyamines with the different chemical and electronic structures. We used spherical gold nanoparticles coated by organic protective and stabilizing layer to prevent the direct interaction between gold surface with alkoxyamines. The analysis of the reaction rates allows us to prove the importance of the electronic features of organic molecules in plasmon-assisted transformations.

Results of previous investigation of the plasmonic homolysis of AAs and some other molecules^{9, 13, 14} suggested the most probable mechanism of plasmon catalysis is the intermolecular excitation process (3). It includes a direct transition from the highest occupied molecular orbital (HOMO) to the lowest unoccupied molecular orbital (LUMO) of organic molecules initiated by the excited plasmon resonance exhibiting the same or higher energy than the gap between the HOMO and LUMO of a molecule or molecular adsorbate^{14,15} (Fig. 1A). The most frequent illustration of this mechanism includes the location of Fermi level of plasmonic nanostructure between HOMO and LUMO; however, a more common situation for organic reagents implies HOMO, LUMO levels of energy which are far above or below the Fermi level^{19,20} It means that we have to consider organic molecules with a different structure for the detailed study of plasmon mechanistic aspects. Therefore, here we selected alkoxyamines with different structures to consider their plasmon-induced homolysis due to the simplicity of kinetic measurement using sensitive EPR methods.

Results and Discussion

AuNPs-C₄H₉: plasmonic system characterization

Here, we commenced our investigation with the preparation of spherical gold nanoparticles (AuNPs) sized 14.3 ± 2 nm modified by lipophilic functional groups (FGs) are prepared via diazonium chemistry (Fig. S1 and Fig. 1B), giving AuNPs-C₄H₉. The organic coating prevents the direct interaction between orbitals of gold with the π -electrons in alkoxyamines structure as back π -donation causes weakening energy required for C–ON bond homolysis.⁹ Moreover, the lipophilic nature of AuNPs-C₄H₉ leads to their stabilization in toluene for further plasmonic experiments with EPR monitoring. The scope of AAs with various substituents in the alkyl and nitroxyl parts (TEMPO-St-NH₂, SG1-St-NH₂, NH₂-TEMPO-St, TEMPO-St-COOEtNH₂, TEMPO-Pyr) (Fig. 1E) was used for the mixing with AuNPs-C₄H₉ in toluene and the further illumination with LED with 660 nm (Fig. 1D) corresponding to the maximum of plasmon resonance in toluene. The illumination at the plasmon resonance of AuNPs-C₄H₉ triggers the C-ON bonds homolysis and the subsequent generation of nitroxide, which can be precisely and quickly detected by EPR (Fig. 1B). EPR provides information about the nature and number of radicals leading to careful kinetic measurements.

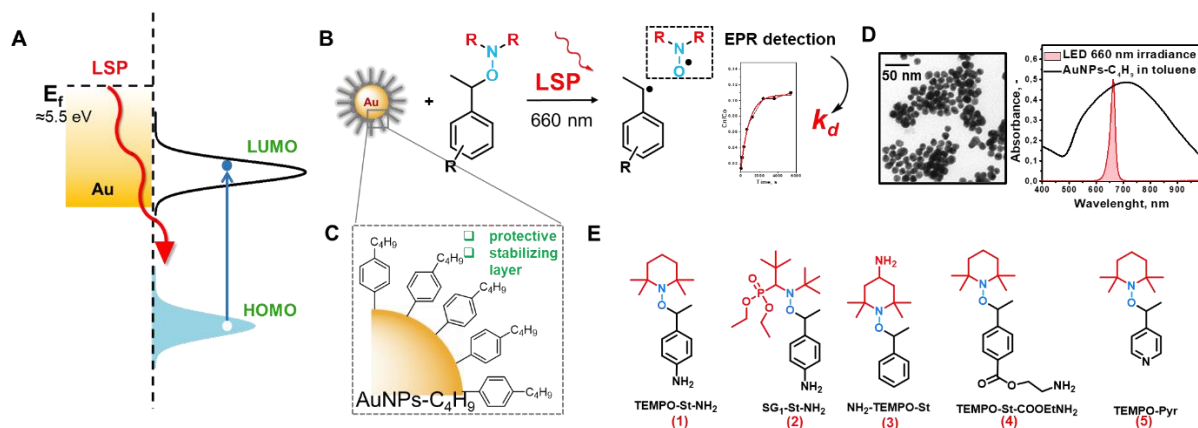


Figure 1. Overview of the experimental strategy. **A** - Scheme for the direct intramolecular excitation mechanism via localized surface plasmon (LSP) resonance and location of HOMO, LUMO levels, **B** -

Scheme of plasmon-induced homolysis of alkoxyamines using AuNPs-C₄H₉, **C** - the structure of organic layer, **D** -TEM image, and UV-Vis spectra of AuNPs-C₄H₉, **E**- structures of alkoxyamines investigated.

Optimization C(AuNPs)/C(AA) ratio and plasmonic homolysis

In order to develop the most reliable system AuNPs-C₄H₉ -AA for the monitoring of plasmon-induced homolysis kinetic, we varied the weight ratio of concentration in AuNPs and alkoxyamines C(AuNPs)/C(AA) from 0.05 to 41 (Fig. S2). The conversion was growing with the C(AuNPs)/C(AA) weight ratio, the ratio 41 was found to be optimal due to the full conversion of AA and high convergence to a linear function. The further increase of C(AuNPs)/C(AA) ratio led to the aggregation (Fig. S2D) of AuNPs-C₄H₉ with limiting the optical properties and homogeneity of the probe.

Kinetic study of plasmon-induced AA homolysis

Using optimal conditions, we performed the plasmon-induced homolysis of 10⁻⁴ M solutions of TEMPO-St-NH₂, SG₁-St-NH₂, NH₂-TEMPO-St, TEMPO-St-COOEtNH₂, TEMPO-Pyr in the presence of AuNPs-C₄H₉. During the homolysis, we analyzed probes taken after certain periods by EPR analysis, where the intensity of signal corresponds to the number of radical species. Recorded EPR signal (Fig. S3) provide kinetic data (Fig. 2A), where the plasmon induced homolysis was fitted with 1st order kinetic equation. The values of k_d (Fig. 2C) are estimated by fitting the plots of concentration vs. time with equation (1)

$$\frac{[\text{nitroxide}]_t}{[\text{nitroxide}]_\infty} = 1 - \exp^{-k_d \cdot t} \text{ eq (1)}$$

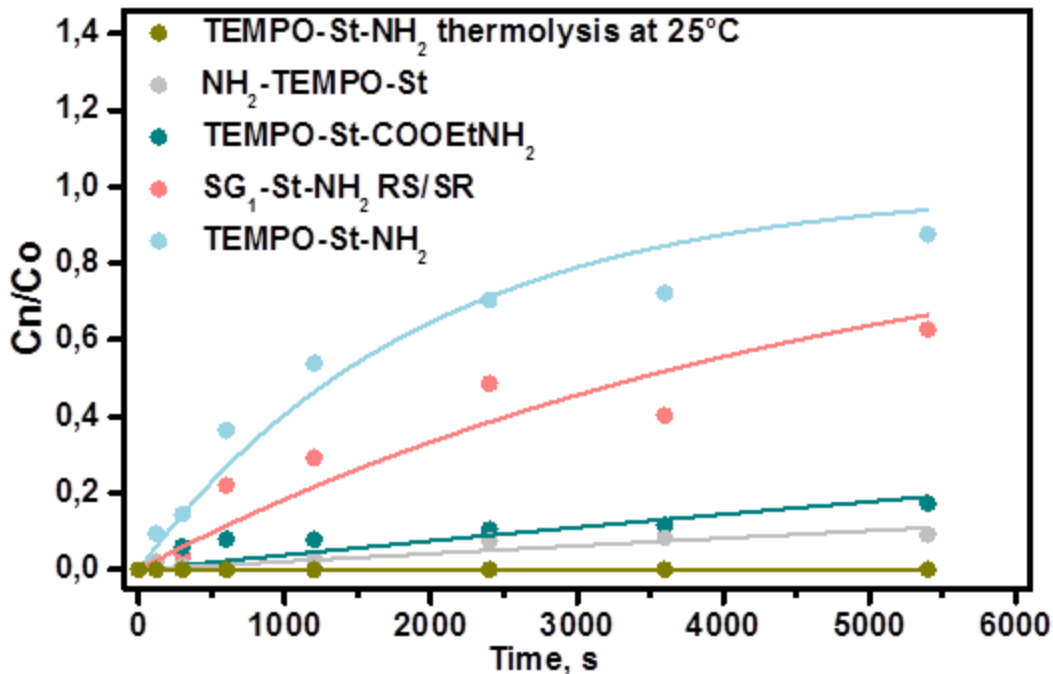


Figure 2. EPR kinetic curves of AAs (0.1mM stock solution of appropriate alkoxyamines) in the presence of AuNPs-C₄H₉ in weight ratio C(AuNPs-C₄H₉)/C(AA) = 41 under LED 660 nm irradiation and thermolysis of TEMPO-St-NH₂ at 25 °C

Table 1. Kinetic data of AAs homolysis of k''_d at 100 °C, k'_d at 25 °C, and k_d at 25 °C under light illumination, activation energies E_a , temperature expected T_p , and energy of HOMO E_{HOMO}

Compound	PI-		k''_d, s^{-1} at 100 °C ^c	$E_a, kJ mol^{-1}$	$T_p, °C^d$	E_{HOMO}, eV^e
	homolysis ^{a,b}	k'_d, s^{-1} at 25 °C ^c				
	k_d, s^{-1}					
(1)TEMPO-Pyr	$3.5 \cdot 10^{-9f}$	$3.5 \cdot 10^{-9}$	$1.3 \cdot 10^{-4}$	130.3 ^g	-	-5.72
(2)NH ₂ -TEMPO-St	$2.1 \cdot 10^{-5}$	$8.8 \cdot 10^{-10}$	$4.5 \cdot 10^{-5}$	133.7	95	-5.25

(3)TEMPO-COOEtNH ₂	3.9·10 ⁻⁵	3.2·10 ⁻⁹	1.3·10 ⁻⁴	130.5	91	-5.38
(4)SG1-St-NH ₂	2.0·10 ⁻⁴	1.7·10 ⁻⁸	4.9·10 ⁻⁴	124.5 ^h	93	-5.18
(5)TEMPO-St-NH ₂	5.2·10 ⁻⁴	1.5·10 ⁻⁸	4.4·10 ⁻⁴	127.3 ^g	103	-5.05

^a Plasmon-induced homolysis was performed at room temperature in toluene in ratio C(AuNPs-C₄H₉) / C (alkoxyamine)= 41.

^b Rate constant k_d was calculated from eq. 1. ^c k_d values were calculated from eq. 2. ^d Estimated T_p assuming a pure thermal effect for the plasmon effect as given in eq. 3. ^e HOMO energy were estimated from CVA (See FigS4). ^f In the worse case, plasmon effect cannot be differentiate from the thermal effect. As no homolysis was observed, thermal value of k'_d at 25 °C was used. ^g See ref. 21. ^h See ref. 9. ⁱ See ref. 22.

$$k'_d \text{ or } k''_d = 2.4 \cdot 10^{14} \cdot \exp\left(\frac{-E_a}{R \cdot T}\right) \quad (\text{eq.2})$$

During 6000 s illumination of TEMPO-St-NH₂, SG1-St-NH₂, with AuNPs-C₄H₉ at 660 nm, we noted fast growth of radical concentration in the first \approx 500 s (1), and a plateau of nitroxide concentration was reached in less than 3000 s. The k_d values of TEMPO-St-NH₂ and SG1-St-NH₂ were measured to be $5.2 \cdot 10^{-4} \text{ s}^{-1}$ and $2 \cdot 10^{-4} \text{ s}^{-1}$, respectively, exhibiting a 3.6 times difference, while thermal homolysis at 100 °C for these AA occurs at approximately the same rate ($4.4 \cdot 10^{-4} \text{ s}^{-1}$ and $4.9 \cdot 10^{-4} \text{ s}^{-1}$). The most active TEMPO-St-NH₂ was homolyzed 10^4 faster under plasmon excitation on AuNPs-C₄H₉ than at room temperature. While for NH₂-TEMPO-St, TEMPO-St-COOEtNH₂ the plasmon-induced homolysis occurred one order of magnitude slower, with k_d $3.9 \cdot 10^{-5} \text{ s}^{-1}$ and $2.1 \cdot 10^{-5} \text{ s}^{-1}$, respectively, than for TEMPO-Sty-NH₂ and SG1-Sty-NH₂. In sharp contrast to TEMPO-sty-NH₂ and SG1-sty-NH₂, the thermal-derived kinetic constants k'_d at 100 °C ($4.5 \cdot 10^{-5}$ and $1.3 \cdot 10^{-4} \text{ s}^{-1}$, respectively) for these AAs differ significantly with k_d (plasmon). In case of TEMPO-Pyr the signal of nitroxide is not detected up to 5000 s of plasmonic homolysis, while thermal homolysis easily proceeds at 100 °C, i.e., complete conversion of AA into nitroxide. To get a holistic picture, we compared k_d and k'_d or k''_d of all AAs obtained from plasmon and thermal homolysis,

respectively, and did not find the convergence suggesting some alternative explanation of plasmonic AA homolysis.

Previously, we developed a procedure for the estimation of apparent temperature T_p as a descriptor of temperature that can “provide” plasmon at normal conditions using E_a values⁹ according to equation (2) (Fig. 2D). Briefly, E_a was calculated using k_d (thermal homolysis, see SI) and averaged factor A^{23} while T_p was calculated as given by eq. 3 using E_a and k_d (plasmon).

$$T_p = \frac{E_a}{R \cdot \ln \frac{2.4 \cdot 10^{14}}{k_d(\text{plasmon})}}. \quad (\text{eq. 3})$$

The values of T_p for five different AAs were not correlated with k_d , k'_d and k''_d and varied from 91 to 103 °C. Additional, the absence of trends between k_d and k''_d (Fig. 4A) leads us to discard the occurrence of thermal effect and a straightforward correlation of the plasmon-triggered homolysis event with the factors governing the thermal homolysis. These results one more time challenges the key role of plasmonic heating and provokes us to consider chemical factors. For example, the polar, steric, and stabilization effects,^{24,22} and hydrogen bonds²⁵ were previously considered as affecting kinetic factors, while effects from all these factors can be merged in the chemical and electronic structure of AA (different location of HOMO and LUMO levels). Therefore, we experimentally measured HOMO and LUMO energies using cyclic voltammetry and UV-Vis data (Fig. S4 and Table S4.1). We attempted to find correlations with energy gap (E_{gap}), HOMO and LUMO levels, E_{HOMO} and E_{LUMO} , respectively (Figure 3B-D). The trend of k_d which increases from **1** to **5** is not observed for k''_d , E_{gap} and E_{LUMO} (Figure 3), whereas it is observed for E_{HOMO} . On the other hand, a good linear dependence with $R^2=0.97$ is observed for the trend of k_d and E_{HOMO} which is confirmed by correlation between $\log k_d$ vs E_{HOMO} (Figure 3D).

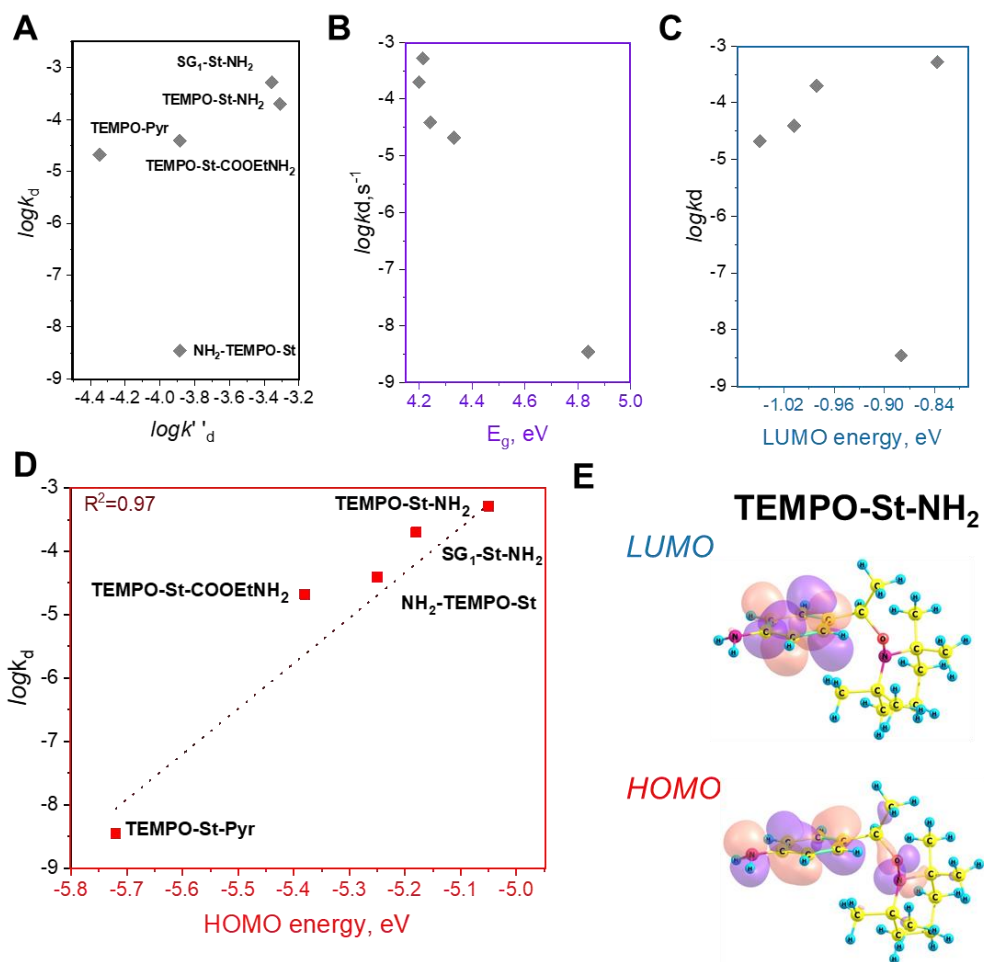


Figure 3 Trends of $\log k_d$ (plasmon) vs **A** - $\log k'_d$ (at 100 °C), **B** - E_{gap} , **C** - E_{LUMO} , **D** - E_{HOMO} , and **E** - Contour plots for the HOMO and LUMO molecular orbitals for TEMPO-St-NH₂

Challenging three mechanisms of plasmon catalysis for AAs homolysis

The changes in k_d and T_p depending on the structures of AA as well as the different trends observed led us to reconsider carefully the three common mechanisms of plasmon catalysis invoked to describe the reactivity observed (Figure 4), namely, plasmonic heating (Figure 4.1), hot electrons (Figure 4.2) and direct intramolecular excitation (Figure 4.3).

The “plasmonic heating” is one of the most frequent mechanism^{26,27} however, the non-correlation between k_d and k'_d , (Fig. 4A) and difference in T_p clearly highlight a minor occurrence of process (1) in

the homolysis of the C—ON bond. The temperature of the experimental system can be decomposed into macroscopic collective effects, measurable with a thermocamera, and local overheating of nanoparticles, calculated theoretically (Fig. S6). Performed calculations using Generalized Multiparticle Mie theory revealed that under our experimental conditions, local heating in the vicinity of AuNPs is on the order of 10^{-3} °C (Fig. S5A, B). Measurements of temperature during plasmon induced homolysis were performed in the reaction vessel with AuNPs-C₄H₉+TEMPO-St-NH₂ in toluene under 660 nm LED illumination and thermal camera FLIR ETS320. After 6000 s illumination, the increase of the reaction temperature in the middle of reaction vessel was found to be 6 ± 3 °C (Fig. S6C, D). Taking into account homolysis temperatures for all AAs is larger than 60 °C^{9,21, 22} such change in temperature is considered to be insignificant. Moreover, the increase in temperature of AuNPs-C₄H₉+TEMPO-St-NH₂ under illumination was found to be linear ($R^2=0.96$) (Fig. S6C): light absorption is proportional to the optical power impinging onto the sample.²⁸ The case of a photothermal process is, however, different and should not feature such a linear dependence.²⁸ To get close mechanistic inside, the variation of LED power from 0-409 mW/cm² for the same system demonstrates highly super linear dependence with $R^2_{lin}= 0.99$ (Fig. S6), leading us to discard such effect. Indeed, closer fitting of power dependence to the linear rather than exponential increase is a signature of the absence of photothermal effects. However, the maximum LED power 409 mW/cm² lead to the deviation toward a super-linear dependence probably to previously described multiphoton absorption.²⁹ If to consider the maximum power, coefficient R^2_{lin} and R^2_{Arr} become 0.74 and 0.73, respectively, suggesting low convergence with each function.

In the hot electron excitation mechanism (2), electrons with a specific energy are resonantly transferred from metal to the LUMO states resulting in the formation of anionic species, which have not been detected by EPR spectroscopy. This scenario is less probable for plasmon-induced AAs homolysis because the transfer is occurring between Au and LUMO level while k_d of homolysis does not depend on E_{LUMO} . In case of electron transfer, the formation of radical anion of AA is expected and one of the mesolysis pathway affords TEMPO and benzylic-type anion (Fig. S7). The reaction pathway was studied via GCMS

in the presence of non-degassed Methanol- d_4 as scavenger of anions. However, the expected 4-(ethyl-1- d)aniline was not observed highlighting the absence of anionic species, which excludes mesolysis process. The experimental results is one more argument against the occurrence of hot electrons mechanism in the plasmon-triggered decomposition of AA.

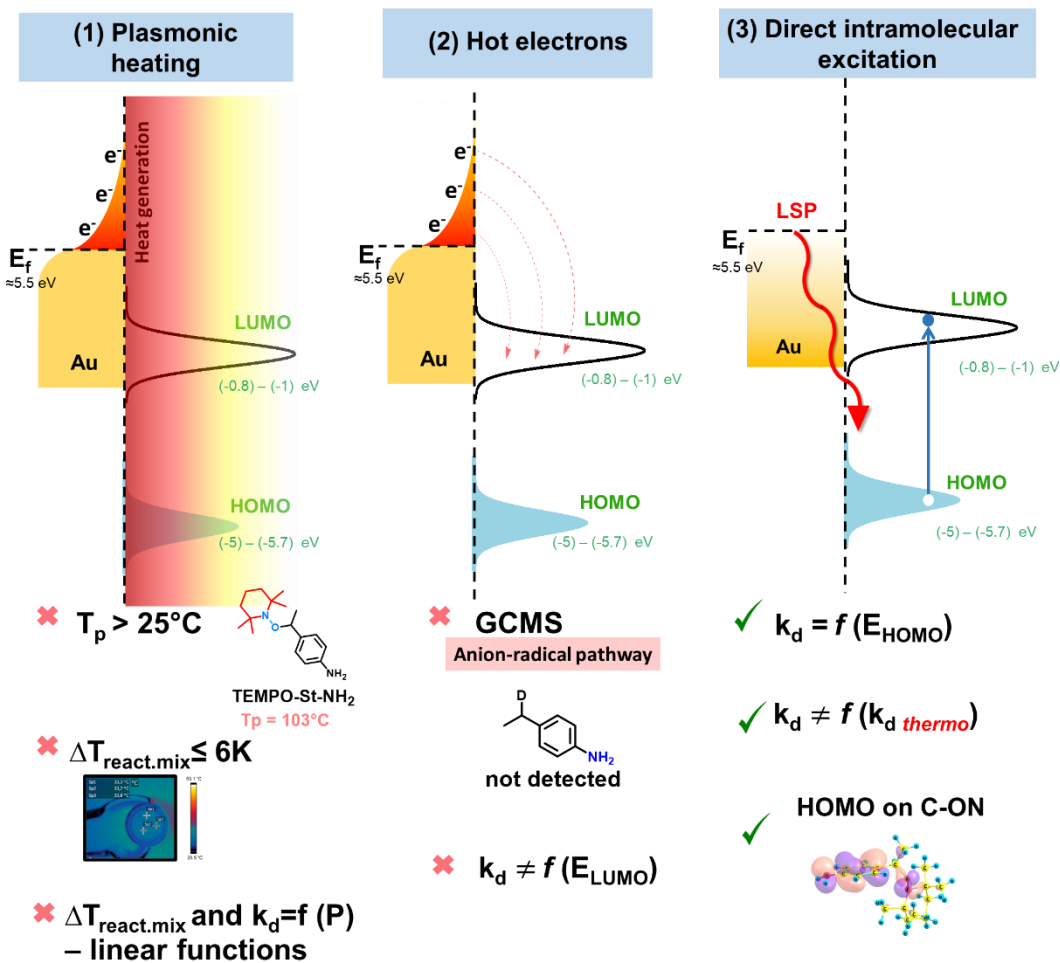


Figure 4. Overview of three possible mechanisms and arguments for/against each of mechanisms: 1) plasmonic heating (2) transfer of a «hot» carriers to the organic molecule, followed by the formation and relaxation of the excited state; (3) intramolecular excitation of an electron to the LUMO via the decay SP.

Finally, the mechanism (3) of intramolecular excitation is the sole, which includes the interaction of electronic orbital HOMO with optically excited surface plasmon. The dependence of the k_d (plasmon) values on the HOMO level suggests that plasmon-induced homolysis of alkoxyamines occurs according to

the mechanism of intramolecular excitation (Fig. 4). We also calculated the localization of HOMO and LUMO over the AA molecules (Table S4.2, Fig. S3E): only HOMO electron densities are localized on the nitroxyl part of all AA while LUMO is not (contour plots in Tab S4.2) suggesting the critical role of HOMO orbitals in plasmonic homolysis. In our case, in the proximity of the AuNPs-C₄H₉ surface, the electronic structure and bond energies in the AAs can be altered significantly with the formation of AuNPs-AA conjugate. Therefore, we investigate AuNPs-C₄H₉-AA conjugates using UV-Vis spectroscopy. The excitation of these conjugates may play a crucial role to account for the difference in homolysis rate k_d reported in Table 1. However, we have to notice here, that AuNPs are coated by 1.8 nm thick polyphenylene layer, which serve as protecting against any direct chemical interactions with gold surface. Moreover, the usage of toluene solvent prevents the hydrophobic-hydrophobic interactions between AuNPs-C₄H₉ and AA. AuNPs-C₄H₉ in toluene were mixed with AAs solution, left for interaction and UV-Vis spectra were recorded. In case of all AAs, we observed the shift of the maximum of plasmon resonance of AuNPs-C₄H₉ (Fig. 2A, S8) for all AA. Further **AuNPs-C₄H₉** + AAs are excited using 660 nm LED (denoted in Fig. S8A), where there is almost equal absorbance for all AAs (Fig. S8B). Obtained data suggest that the difference in the homolysis rate is not because of different interaction with AuNPs-C₄H₉ but electronic structure of AA. Summing up, clear dependence $k_d(\text{plasmon})=f(\text{HOMO})$ not from LUMO, localization of electron density of HOMO on C-O bonds and correlation of electronic structures of AAs with plasmonic **AuNPs-C₄H₉** and k_d are convincing that the key mechanism of intramolecular excitation for plasmon-induced AA homolysis (Fig. 4.3). One can wonder if the energy of plasmon excitation is enough to get 100% conversion of AA according to mechanism (4.3) (presented in Figure 4.3), as the energy gap for TEMPO-St-NH₂ is ≈ 5 eV, while 660 nm light corresponds to the 1.8 eV. The dependences of the reaction rate on the incident optical power offer the multiphoton adsorption/ two-stage absorption may occur at 409 mW/cm² (Fig. S6) and provide energy multiplication to overcome the energy gap of AAs²⁸.

Conclusion

In summary, we used alkoxyamines as a plasmonic probe (due to one component reaction with 1st order kinetics) mixed with AuNPs coated by protective/stabilizing layer for the study of plasmon induced homolysis under plasmon excitation using EPR monitoring. The detailed kinetic study with optimal experimental conditions revealed the differences in kinetic parameters of homolysis k_d (plasmon) and k''_d (thermal) and T_p of different AAs, which cannot be explained by the activation energies of AAs and one more time challenge the key role of plasmonic heating and provoke us consider chemical factors. All investigations – kinetics by EPR, SERS and UV spectroscopies for adsorption, TDFTD for orbitals calculations, cyclic voltammetry for determination of HOMO-LUMO energies, GC-MS for product analysis – concur at promoting the direct intramolecular excitation mechanism (3) to account the triggered-plasmon catalytic homolysis of AA at room temperature and to discard the occurrence of plasmonic heating and hot electron transfer events. Therefore, amongst the three main mechanisms of plasmon catalysis, we discard both the plasmonic heating (process (1)) due to $k_d \neq f(k''_d)$, to the absence of heating and to the power variation experiments, and the electron transfer (process (2)) due absence of anionic species and to the LUMO energy involvements and to the absence of anion radical products (not detected by GC-MS). Dependence of k_d (plasmon) on the HOMO energy, localization of electron density of HOMO mainly are convincing the key mechanism of intramolecular excitation for plasmon-induced AA homolysis. Our study supports the importance of the chemical and electronic structure of reagents for the plasmon-induced catalysis. We believed that these findings would convince plasmonic chemists to consider photochemical reaction from different points of views - physical as well as chemical.

Methods

General procedure for kinetic measurements

A suspension of AuNPs-C₄H₉ and solution of alkoxyamine in toluene 0.01 mM were mixed with ratio C(AuNPs-C₄H₉)/C(AA) 40 to 1 in an NMR tube, treated with ultrasound, and irradiated with a LED (660 nm, 409 mW/cm²; Thorlabs) from bottom to top. LED was closed to the tube without any distance. For kinetic measurements, the NMR tube was removed from the irradiation source and placed into an ESR

cavity thermostated at 25 °C. After ESR spectra were recorded, and the NMR tube was removed from the ESR cavity and again irradiated by the LED under the same conditions. Sampling was made several times in various periods to plot kinetic curve.

Acknowledgements

This work was supported by Tomsk Polytechnic University VIU-RSCABS-194/2020 (the kinetic evaluation of homolysis and preparation of NPs) and Russian Science Foundation (№ 20-73-00236 for the preparation of alkoxyamines). R. R. V. thanks the Academy of Finland (projects 1325369, 1315600)

Competing interests

The authors declare no competing interests.

References

1. Carter, P., Martirez, J. M. P., Bao, J. L. & Carter, E. A. First-Principles Insights into Plasmon-Induced Catalysis. 1–21 (2020).
2. Zhang, Z., Zhang, C., Zheng, H. & Xu, H. Plasmon-Driven Catalysis on Molecules and Nanomaterials. *Acc. Chem. Res.* **52**, 2506–2515 (2019).
3. Adleman, J. R., Boyd, D. A., Goodwin, D. G. & Psaltis, D. Heterogenous catalysis mediated by plasmon heating. *Nano Lett.* **9**, 4417–4423 (2009).
4. Hou, W. & Cronin, S. B. A review of surface plasmon resonance-enhanced photocatalysis. *Adv. Funct. Mater.* **23**, 1612–1619 (2013).
5. Gellé, A. *et al.* Applications of Plasmon-Enhanced Nanocatalysis to Organic Transformations. *Chemical Reviews* vol. 120 986–1041 (2020).
6. Erzina, M. *et al.* Plasmon-Assisted Transfer Hydrogenation: Kinetic Control of Reaction

- Chemoselectivity through a Light Illumination Mode. *J. Phys. Chem. C* **125**, 10318–10325 (2021).
7. Miliutina, E. *et al.* Can Plasmon Change Reaction Path? Decomposition of Unsymmetrical Iodonium Salts as an Organic Probe. *J. Phys. Chem. Lett.* **11**, 5770–5776 (2020).
 8. Zhang, X. *et al.* Plasmon-Enhanced Catalysis: Distinguishing Thermal and Nonthermal Effects. *Nano Lett.* **18**, 1714–1723 (2018).
 9. Guselnikova, O. *et al.* Establishing plasmon contribution to chemical reactions: alkoxyamines as a thermal probe. *Chem. Sci.* **12**, 4154–4161 (2021).
 10. Guselnikova, O. *et al.* Plasmon-assisted click chemistry at low temperature: an inverse temperature effect on the reaction rate. *Chem. Sci.* **12**, 5591–5598 (2021).
 11. Sytwu, K., Vadai, M. & Dionne, J. A. Bimetallic nanostructures: combining plasmonic and catalytic metals for photocatalysis. *Adv. Phys. X* **4**, (2019).
 12. Nazemi, M., Panikkanvalappil, S. R., Liao, C.-K., Mahmoud, M. A. & El-Sayed, M. A. Role of Femtosecond Pulsed Laser-Induced Atomic Redistribution in Bimetallic Au–Pd Nanorods on Optoelectronic and Catalytic Properties. *ACS Nano* **15**, 10241–10252 (2021).
 13. Kazuma, E. & Kim, Y. Mechanistic Studies of Plasmon Chemistry on Metal Catalysts. *Angew. Chemie Int. Ed.* **58**, 4800–4808 (2019).
 14. Kazuma, E., Jung, J., Ueba, H., Trenary, M. & Kim, Y. Plasmon-induced chemical reaction of a single molecule. *Science (80-.)*. **526**, 521–526 (2018).
 15. Kookhaee, H., Tesema, T. E. & Habteyes, T. G. Switching a Plasmon-Driven Reaction Mechanism from Charge Transfer to Adsorbate Electronic Excitation Using Surface Ligands. *J. Phys. Chem. C* **124**, 22711–22720 (2020).
 16. Kazuma, E., Jung, J., Ueba, H., Trenary, M. & Kim, Y. Direct Pathway to Molecular

- Photodissociation on Metal Surfaces Using Visible Light. *J. Am. Chem. Soc.* **139**, 3115–3121 (2017).
17. Mo, J. *et al.* Atomic-Precision Tailoring of Au–Ag Core–Shell Composite Nanoparticles for Direct Electrochemical-Plasmonic Hydrogen Evolution in Water Splitting. *Adv. Funct. Mater.* **2102517**, 1–11 (2021).
 18. Guselnikova, O. *et al.* Unprecedented plasmon-induced nitroxide-mediated polymerization (PI-NMP): A method for preparation of functional surfaces. *J. Mater. Chem. A* **7**, 12414–12419 (2019).
 19. Vega-Peñalozza, A., Mateos, J., Companyó, X., Escudero-Casao, M. & Dell’Amico, L. A Rational Approach to Organo-Photocatalysis: Novel Designs and Structure-Property Relationships. *Angew. Chemie - Int. Ed.* **60**, 1082–1097 (2021).
 20. Fraser, J. P. *et al.* Application of a 2D Molybdenum Telluride in SERS Detection of Biorelevant Molecules. *ACS Appl. Mater. Interfaces* **12**, 47774–47783 (2020).
 21. Nkolo, P. *et al.* C-ON bond homolysis of alkoxyamines: When too high polarity is detrimental. *Org. Biomol. Chem.* **15**, 6167–6176 (2017).
 22. Audran, G., Brémond, P., Joly, J. P., Marque, S. R. A. & Yamasaki, T. C-ON bond homolysis in alkoxyamines. Part 12: The effect of the para-substituent in the 1-phenylethyl fragment. *Org. Biomol. Chem.* **14**, 3574–3583 (2016).
 23. Walton, J. C. *Analysis of Radicals by EPR. Encyclopedia of Radicals in Chemistry, Biology and Materials* (2012). doi:10.1002/9781119953678.rad001.
 24. Marque, S., Fischer, H., Baier, E. & Studer, A. Factors influencing the C-O bond homolysis of alkoxyamines: Effects of H-bonding and polar substituents. *J. Org. Chem.* **66**, 1146–1156 (2001).
 25. Audran, G. *et al.* How intramolecular hydrogen bonding (IHB) controls the C-ON bond homolysis

- in alkoxyamines. *Org. Biomol. Chem.* **15**, 8425–8439 (2017).
26. Dubi, Y., Un, I. W. & Sivan, Y. Thermal effects - an alternative mechanism for plasmon-assisted photocatalysis. *Chem. Sci.* **11**, 5017–5027 (2020).
 27. Sivan, Y., Baraban, J., Un, I. W. & Dubi, Y. Comment on “Quantifying hot carrier and thermal contributions in plasmonic photocatalysis”. *Science* vol. 364 (2019).
 28. Baffou, G., Bordacchini, I., Baldi, A. & Quidant, R. Simple experimental procedures to distinguish photothermal from hot-carrier processes in plasmonics. *Light: Science and Applications* vol. 9 2047–7538 (2020).
 29. Olsen, T. & Schiøtz, J. Origin of Power Laws for Reactions at Metal Surfaces Mediated by Hot Electrons. *Phys. Rev. Lett.* **103**, 1–4 (2009).